Biosensors and Bioelectronics 166 (2020) 112426

Contents lists available at ScienceDirect

Biosensors and Bioelectronics

journal homepage: http://www.elsevier.com/locate/bios

# Flexible and water-stable graphene-based electrodes for long-term use in bioelectronics

G. Murastov [a], E. Bogatova [a], K. Brazovskiy [a], I. Amin [b], A. Lipovka [a], E. Dogadina [a], A. Cherepnyov [a], A. Ananyeva [a], E. Plotnikov [a], V. Ryabov [c], R.D. Rodriguez [a,*], E. Sheremet [a,**]

[a] Tomsk Polytechnic University, Lenina ave. 30, 634034, Tomsk, Russia
[b] Van't Hoff Institute of Molecular Science, University of Amsterdam, Science Park 904, 1098XH, Amsterdam, Netherlands
[c] Cardiology Research Institute, Tomsk National Research Medical Center, 111a Kievskaya Street 634012, Tomsk National Research Tomsk State University, 36 Lenina ave 634050, Siberian State Medical University, 2 Moscovskiy trakt, 634050, Tomsk, Russia

ARTICLE INFO

*Keywords:*
Bioelectrodes
2D materials
Reduced graphene oxide
Laser processing
Laser-reduction
Cardiography
TOC graph

ABSTRACT

We present the first demonstration of bioelectrodes made from laser-reduced graphene oxide (rGO) on flexible polyethylene terephthalate (PET) substrates that overcome two main issues: using hydrogel on skin interface with standard Ag/AgCl bioelectrodes *vs*. low signal to noise ratio with capacitance or dry electrodes. Today we develop a dry rGO bioelectrode technology with long-term stability for 100 h in harsh environments and when in contact with skin. Reliability tests in different buffer solutions with pH from 4.8 to 9.2 tested over 24 h showed the robustness of rGO electrodes. In terms of signal to noise ratio, our bioelectrodes performance is comparable to that of commercial ones. The bioelectrodes demonstrate an excellent signal to noise ratio, with a signal match of over 98% with respect to state-of-the-art electrodes used as a benchmark. We attribute the unique stability of our bioelectrodes to the rGO/PET interface modification and composite formation during laser processing used for GO reduction. The rGO/PET composite formation assertion is confirmed by mechanical stripping experiments and visual examination of re-exposed PET. The method developed here is simple, cost-effective, maskless, and can be scaled-up, allowing sustainable manufacture of arbitrary-shaped flexible electrodes for biomedical sensors and wearables.

## 1. Introduction

Bioelectrodes are deeply embedded in medicine, widely used in diagnostics and health monitoring (electrocardiography (ECG) (Shahandashti et al., 2019), electroencephalography (EEG) (Gan et al., 2020), ballistocardiography and sleep monitoring (Meng et al., 2020; Zhou et al., 2020). Other applications include smart-textiles as skin conductors (Chen et al., 2020; Zhang et al., 2020, 2018; Zou et al., 2019), cardiac therapy (Liu et al., 2019; Ouyang et al., 2017), and chemical body sensors including pH meters (Webster, 2006). Although conventional electrodes (Ag/AgCl) demonstrate high stability, reproducibility, and are suitable for both ECG and impedance measurements (Li et al., 2017), long-term exposure to silver-containing products can lead to localized topical argyria (blue discoloration due to the accumulation of silver sulfides) (Beutler BD, n.d.). Besides, the adhesive layer attaching the electrode to the skin may cause allergic reactions, trigger bacterial growth, and induce skin irritation (Uter et al., 2018). Moreover, the skin under the adhesive layer sweats over time, resulting in surface degradation that worsens signal detection and recording of results (Searle and Kirkup, 2000). These are significant issues that affect the development of future wearable electronic sensors and devices that require constant and reliable signal monitoring. For instance, atrial fibrillation (AF), which is the most common arrhythmia type, does not show any symptoms. Meanwhile, the frequency of asymptomatic AF cases detection varies from 10% to 40% ((chair) et al., 2017). The chance to successfully detect heart disease in this case directly depends on the duration of ECG monitoring as shown by Sanna et al. and Gladstone et al. studies (Gladstone et al., 2014; Sanna et al., 2014). Therefore, only electrodes with safe, comfortable, and stable long-term performance are appropriate. That makes traditional Ag/AgCl electrodes existing for more than 40 years ill-suited for further development of biocompatible wearable electronics (Chlaihawi et al., 2018).

* Corresponding author.
** Corresponding author.
*E-mail addresses:* raul@tpu.ru (R.D. Rodriguez), esheremet@tpu.ru (E. Sheremet).

https://doi.org/10.1016/j.bios.2020.112426
Received 15 March 2020; Received in revised form 29 June 2020; Accepted 2 July 2020
Available online 11 July 2020

The main reason why conventional electrodes are not an option for long-term monitoring is the necessity to use additional conductive gels. The gel reduces the electrical resistivity of the epidermis making its dry outer layer ion conductive, but it also may cause an allergic reaction and decrease signal quality, dry out with long-term use (Scheman et al., 2019; Tiwari, 2017).

In this regard, the development of new "dry" biosensors for long-term ECG monitoring is critical (Steinberg et al., 2019). Compared to wet bioelectrodes, the dry ones allow performance without the need for gel or skin pretreatment. This results in lower impedance changes, lower noise, and better signal stability (Searle and Kirkup, 2000; Zhou et al., 2013). There are various demonstrations of dry bioelectrodes, for example, Ag:TiN nanocomposite, where TiN is a biocompatible and electrically conductive ceramic with excellent chemical stability and mechanical properties (Pedrosa et al., 2014); dry silver bioelectrodes such as conductive foam coated with a layer of silver by thermal evaporation; and flexible printed silver-ink electrodes (Casson et al., 2017). Other alternatives to Ag/AgCl electrodes include microstructured dry bioelectrodes based on conductive liquid silicone rubber (LSR) and capacitive bioelectrodes made on silicone with thermally grown silicon dioxide as a dielectric layer. These electrodes have a much lower contact impedance, which provides a high-quality recording of biopotentials (Gruetzmann et al., 2007; Kaitainen et al., 2014; Searle and Kirkup, 2000; Zhou et al., 2013). However, a limitation of dry electrodes is the non-Ohmic contact interface, which makes them work as a capacitor when in contact with skin. Besides, dry electrodes require special measures to remove DC polarization. Although they are very stable for a couple of hours, after that, polarization effects start taking place and the electrode/skin interface becomes very sensitive to almost all possible interfering factors (Ask et al., 1979).

Carbon materials are promising candidates to serve as dry bioelectrodes platforms while at the same time overcoming the issues mentioned above. They are easily processed, inexpensive, come in different forms (powders, composites, fibers, *etc.*), have high strength and surface area, excellent mechanical resistance, and high electrical and thermal conductivity (Maiti et al., 2018). Moreover, carbon materials have relatively passive electrochemistry, the ability to control porosity depending on the activation method, and have electrocatalytically-active sites for various oxidation-reduction reactions making it also possible to control the process of surface electrode renewal to prevent passivation. Carbon-based derivatives are already widely used as bioelectrodes (Taniselass et al., 2019). For example, ethanol-based on graphene sheets of modified electrodes or graphene-based on enzymatic bioelectrodes (Guo et al., 2011; Karimi et al., 2015). All these electrodes show excellent chemical stability and data reproducibility. Another key advantage of carbon materials is the unique properties of their allotropic forms like graphene (Guo et al., 2011; Karimi et al., 2015; Li et al., 2017). Compared to other types of nanomaterials, such as carbon nanotubes and metal nanoparticles, graphene provides a much higher surface area and higher electrocatalytic activity (Karimi et al., 2015). There are several ways to obtain graphene, from mechanical exfoliation of graphite with adhesive tape or in bulk with an industrial mixer (Paton et al., 2014). However, for large-scale processing, graphene is not suitable especially with solution-processable technologies since graphene aggregates in aqueous solutions due to its hydrophobic nature. Besides a lack of water-dispersibility, graphene integration involves high-costs. Therefore, graphene oxide (GO) has come along as a water-dispersible and inexpensive graphene nanomaterial for diverse surface functionalization (Dedelaite et al., 2018; Lipovka et al., 2020) that can be reverted to its graphitic form by chemical, thermal, or photonic reduction (Al-Hamry et al., 2016). This reduction process transforms the insulator GO into an electrically conductive graphene-like material known as reduced graphene oxide (rGO) with a high potential in electronics and sensor applications (Eda et al., 2008; Robinson et al., 2008). However, thermal and chemical reduction have limitations such as high levels of toxicity, hazardousness, risk of explosions, and time-consuming. Photonic reduction by laser irradiation does not suffer from any of these issues, and also offers large-scale fabrication possibilities. This research, pioneered by Kaner's group (Strong et al., 2012), has shown tremendous potential as a key enabling technology for flexible electronics (Gao et al., 2011; Guo et al., 2018; Kuhnel et al., 2019). We found that rGO demonstrates biocompatibility, low-cost processing, and excellent chemical and mechanical stability. These factors are not only crucial for long-term use but also for the realization of robust flexible electrodes (Yun et al., 2017). Moreover, rGO provides an increased density of functional groups, compared to graphene, which facilitates the immobilization of biomolecules and high control over surface properties enabling applications such as the detection of single-cancer cells (Wang et al., 2018). Herein, for the first time, in this work, we demonstrate laser-reduced graphene oxide as a record-performance material for bioelectrodes (see Fig. 1). We propose a one-step fabrication of arbitrary-shaped flexible bioelectrodes based on laser-reduced GO that shows long-term stability at different pH and a prolonged wearing over 100 h demonstrated by *in vivo* studies. Our rGO bioelectrodes processing steps are schematically shown in Fig. 1.

## 2. Materials and methods

### 2.1. GO deposition and reduction

A 4 mg/mL GO dispersion was purchased from Graphenea. A polyethylene terephthalate (PET) sheet of ~ 30x30 × 1 $mm^3$ in size was used as a substrate for GO film deposition following the drop-casting approach without additional treatment except for visual inspection of suspension distribution. However, the simplicity of the method did not limit the film homogeneity or deposition reproducibility as the experimental conditions, including suspension volume and substrate size, were kept the same. 200 and 100 μL of GO were drop-casted on the top and bottom of PET surfaces, respectively (a sketch of bioelectrode construction is presented in Fig. S6). The reason to use different GO volumes on top and back sides is in differences of the area sizes to be covered with suspension. For the bottom electrode, the crucial factor is to form a contact with metal clips, which is 10 mm only, so the amount of material required for that is lower than for the top electrode where the whole disk needs to be covered with GO. Then the sample was carefully dried for 1 h on a heating plate (~60 ℃). GO reduction was performed using a desktop laser engraver with a maximum power of 1 W at a wavelength of 405 nm. Laser diode power density was controlled by adjusting the laser focus on the sample using 3 mm glass plates to raise the sample and prevent sample burning during GO reduction. Measured spot size in the focal plane showed that minimal diameter of the beam could be adjusted down to 15 μm. Patterning was done with the following parameters: zigzag XY-scanning, ~72 μm step, and 100 ms exposure time per step. Regarding the manufacturer, we used generic solid-state laser diodes with no brand, made in China and assembled by NEJE in a laser engraver frame.

### 2.2. Preparation of buffer solutions

Buffer solutions of pH 4.8 and 8 were obtained by mixing solutions of sodium hydrophosphate ($Na_2HPO_4$) and sodium dihydrophosphate ($KH_2PO_4$) in different mixture ratios. The buffer solution with pH 9.2 was prepared by dissolving a titration ampoule in distilled water. For the two-week stability test, a 0.9% NaCl buffer was used.

### 2.3. Stability evaluation in buffer solutions

The electrode stability was investigated using an EEG recording setup Encephalan-131-03 (Medicom MTD Ltd, Research and Development) that allows recording both - biopotential and contact resistance between electrode pairs. This setup is shown in Fig. S1, and was used as a

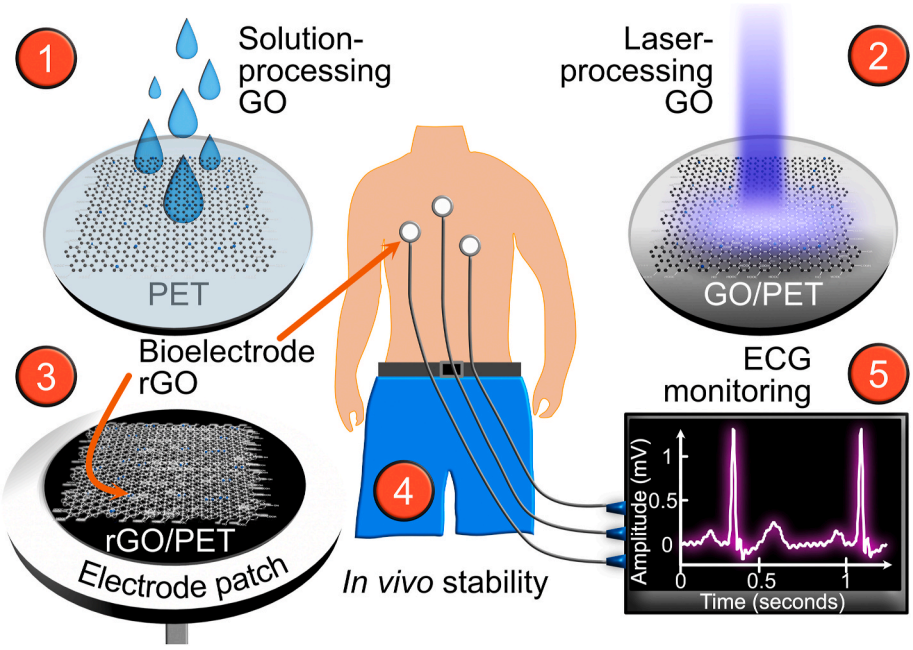


**Fig. 1.** Schematic illustration of the different steps involved in our graphene-based technology for bioelectrodes. 1) Solution processable graphene oxide is used to form films on flexible PET substrates; 2) the GO films are reduced using laser processing and integrated into PET; 3) bioelectrodes are fabricated using the rGO/PET structures attached to a conventional electrode patch with an outer adhesive for skin fixation; 4) continuous wearing rGO bioelectrodes verified stability *in vivo*; 5) ECG monitoring while continuous wearing rGO bioelectrodes without any performance degradation or secondary-effects on the skin up to 108 h.

biopotential measuring device with superior electrical parameters: high-sensitivity, low-noise, and an embedded circuit to continuously measure contact resistance. To measure the electrical characteristics, a conductive contact was created by gluing a copper wire to the rGO structure using conductive silver paste. The assembled electrodes were then immersed in buffer solutions of different pH for 24 h while avoiding contact between the wires and the buffer solution.

### 2.4. Electrical characterization of rGO bioelectrodes

The contact resistance of the electrodes was measured using a four-electrode method. Data acquisition system E−502 (manufactured by L-Card company, www.lcard.ru) was connected to the electrode cell and computer. The excitation AC current with an amplitude of 100 μA and 10 Hz frequency was applied across two current electrodes, while another pair of the electrodes recorded voltage. High precision of 16 bits digital-to-analog converter generated the excitation current, and the voltage was measured by analog-to-digital converter with 10 μV resolution. The estimated signal-to-noise ratio was above 70 dB. In total, there were nine independent 10s long records for each value of pH.

### 2.5. Cell culture methods

Mice-derived embryo fibroblast 3T3-L1 (ATCC CL-173) were cultured in DMEM culture media (BioFroxx, Germany) supplemented with GlutaMAX (cell supplement #35050061, Gibco, TFS), 10% FBS and antibiotics (penicillin/streptomycin mixture, Paneco, Russia). Fibroblasts were cultivated in $CO_2$-incubator (5% carbon dioxide) at 37 °C and used for the experiment when they reached 70% confluence.

### 2.6. Surface cell adhesion and proliferation

All tested electrodes (and PET substrate as a reference) were sterilized by submerging into 70% ethanol solution for 30 min with subsequent 30 min drying in sterile airflow. Then, electrodes were placed individually on a well bottom in a 24-wells plate. Each well was filled with 0.5 mL of 3T3-L1 cells suspension in concentration $10^5$ cell/mL. The plate was placed in a $CO_2$-incubator at 37 °C. We estimated the cell adhesion and growth on electrode surfaces after 24 h of incubation. Since the electrodes are opaque, they had to be stained to visualize the cells. For that, we washed electrodes in phosphate-buffered saline (PBS) solution and placed them in staining solution with Calcein-AM 0.5 μg/mL and Hoechst 33342 1.0 μg/mL (Sigma) for 15 min at 37 °C. The combination of these dyes allowed us to very reliably differentiate living cells growing on the electrode surface from dead cells, physical particles, and other optical artifacts. Then all samples were washed in PBS. This washing procedure introduces the risk of cells removal from the surface in case of poor adhesion or delamination of the top rGO layer. Cells on the surface were visualized by fluorescent microscope Zeiss Axiovert-A1 with LED light sources and appropriate light filter sets. We took photos of three different zones for each electrode in double parallel testing. Obtained images were processed by ImageJ software. We superimposed two channels of images from different dyes and allocated pixel zones corresponding to living cells and summed them up. Final cell densities were recalculated per $mm^2$.

### 2.7. Mechanical stability evaluation using adhesive tape

A GO suspension was drop-casted and subsequently dried on both PET and Kapton (DuPont) substrates. Next, the square-shaped regions were laser engraved on both substrates to form GO/rGO interfaces following the same laser parameters as for bioelectrodes fabrication. A strong adhesive tape (3M™) was attached and stripped away from irradiated and non-irradiated (rGO and GO, respectively) areas.

### 2.8. Contact angle measurements

Contact angle measurements were carried out using DI water to determine if there are any changes in the hydrophobicity of rGO/PET induced by the external environment. The samples were immersed in buffers with pH 1.65, 4.01, 6.86, 9.18 for 48 h except for the control one that remained stored at room conditions. A motorized syringe was used to keep the same volume of a water drop (~8 μL). A short video was recorded to see the spreading tendency of water on the surface. ImageJ software with contact angle plugin was used to evaluate the contact angle values twice, right after deposition, and then 1 min after. For each sample, we repeated the measurement four times to quantify the error and deviation.

### 2.9. Electrodes characterization

*Raman spectroscopy (RS)* was used to track the material chemical composition changes after each treatment. Raman measurements were performed using a DXRTM 2xi Raman Imaging Microscope (785 nm, Thermo Scientific™). The laser power for the pure PET was 15 mW, while for GO and rGO it was limited to 2 mW to prevent sample modification.

*Infrared spectroscopy (IR)* was performed to further confirm and complement the alterations in the chemical composition of rGO bioelectrodes

The IR spectra were recorded in attenuated total reflectance mode using an IR spectrometer (Thermo Smart orbit, Thermo Smart Performer with diamond and germanium crystals, respectively).

*Scanning electron microscopy (SEM)* analysis was done to estimate and track the changes in electrode surface morphology using a dual-beam SEM "Quanta 200 3D", FEI, USA (secondary electron mode, 20kV)

*Optical microscopy unit(Altami, Russia)* was used to routinely inspect changes that occurred at electrode surface after immersion in different pH, and also to investigate the PET surface deformation after cleaning the rGO electrodes using an ultrasonic bath.

### 2.10. In vivo volunteer testing

For the bioelectrode assembly, the Ag/AgCl contact surface with gel was replaced by double-sided rGO disk (18 mm diameter) engraved on PET. The rGO material on different sides contacted the carbon-filled interconnects. One side of this structure has a contact with a metal clip and another was attached to the skin.

Three of the ECG electrodes were rGO-based and the fourth one was a commercial disposable Ag/AgCl electrode, model F9067, purchased from FIAB, Italy. According to Wilson Central Terminal, electrodes were attached at points V1 – Ag/AgCl, V3, V6 - rGO bioelectrodes. The reference electrode based on rGO was located two ribs below V1 point. The same scheme is used in commercially available Holter monitors. The interval between measurement was 12 h and the duration of the test was 108 h. For the ethical reasons we were not allowed to continue the experiment if side effects occurred. The side effects include skin irritation, allergic reactions, degradation of contacting patch of any electrode (Ag/AgCl, GO/rGO or both). According to recommendations of the ethical committee, we should either stop monitoring completely or replace the deteriorated electrodes and provide appropriate measures to eliminate skin irritation. Ag/AgCl electrode was replaced every 36 h to prevent skin irritation and electrode degradation. The rGO electrodes were continuously used for 108 h (4.5 days). Throughout this period, the rGO electrodes were in contact with the skin all the time except for a short interruption to replace the adhesive.

### 2.11. ECG data processing

The ECG data were recorded using a bioamplifier with a high resolution (22 bits) analog-to-digital converter (ADC). The preprocessing step only included removing the DC shift and baseline drift. The digitized and preprocessed ECG samples were stored in European Data Format (EDF) files. There was no additional filtering or power line interference removing, which could possibly mask artifacts in ECG signals caused by the use of our new electrodes. Next, the coefficient of linear correlation was calculated as a measure of similarity between ECG recorded with reference (Ag/AgCl) electrodes and new rGO-based electrodes.

## 3. Results and discussion

### 3.1. rGO reduction

We used the IR spectra from GO/PET and rGO/PET to analyze the changes induced by laser irradiation. The FTIR results are presented in Fig. S2. The spectrum from blank PET is also presented since that was the common substrate for both structures. Taking it into account is important to identify the vibrational modes coming from the actual sample and those arising from the substrate alone. The strong peak at 1720 $cm^{-1}$ represents a carbonyl stretching C═O band, in which peak intensity decreases after laser treatment, indicating the oxygen removal during the reduction process. Peaks at 1240 $cm^{-1}$ and 1186 $cm^{-1}$ are related to asymmetric and symmetric O–C–O vibrations, respectively. GO shows a broad peak from 3000 $cm^{-1}$ to 3670 $cm^{-1}$ corresponding to typical O–H vibrations due to hydroxyl groups from adsorbed water molecules or –OH from phenol or carboxylic groups. This peak disappears after laser processing confirming the partial GO reduction (Strankowski et al., 2016). The GO film microstructure changes before and after laser irradiation were visible in optical microscopy and cross-sectional scanning electron microscopy, as shown in Fig. S3. X-ray photoelectron spectroscopy results (XPS) in Fig. S4 confirmed the changes in GO reduction after laser irradiation supporting the conclusions deduced from IR spectra results. GO survey spectra demonstrate two sharp C1s (285 eV) and O1s (532 eV) peaks, which intensity decreases after laser treatment with O1s/C1s intensity ratio changing from 0.4 to 0.2. The change in the C1s region indicates a significant elimination of C–O bonds giving rise to the C–C peak. The obtained results are in agreement with the previous results obtained for laser-reduced GO on a glass substrate (Rodriguez et al., 2019).

### 3.2. Bioelectrodes water and chemical stability

The rGO bioelectrodes stability was investigated in physiological solution (0.9% NaCl) as an electrolytic model of the body. The average value of contact impedance was ~4 kOhm, however, the absolute value of electrical impedance depends on both the electrodes area and electrochemical environment they are in contact with and does not influence the signal quality. The key point in this regard is that over the two weeks testing period, we did not observe any degradation of electrical conductance. We also recorded the background noise of our electrodes and the Ag/AgCl ones presented in the form of the noise density plot in Fig. S7. Up to 40 Hz, rGO bioelectrodes offer a higher signal/noise ratio than conventional Ag/AgCl electrodes even after long periods of exposure to salt dilutions.

We evaluated the resistance stability of four rGO electrodes in different buffer solutions with pH from 2 to 10. A 24 h test was done to show the dependence of impedance values on pH. The data are presented in Fig. 2a with error bars for each pH level. The average change in contact resistance after the stability test was within the standard deviation range. We observed a monotonic rise of impedance values shifting from acidic (or alkaline) to a neutral environment. A similar behavior could be found for ZnO/rGO or Au/rGO composites (D'Souza et al., 2019; Gugoasa et al., 2019) and GO itself (Lee et al., 2017).

The exact electrochemical mechanisms of contact resistance for GO/rGO electrodes have not been fully studied yet. One of the possible explanations for the contact resistance dependence on pH is that the GO/rGO ratio in the surface layer of the electrodes changes in parallel with pH. It has been reported that the conductivity of GO/rGO composite is a function of this ratio (Gugoasa et al., 2019). In liquid solutions, we also have to take into account the electrical parameters of the double electrical layer between the surface of the electrodes and solution. These effects and their interplay are complex and are the subject of future research.

Li et al.(Li et al., 2011) demonstrated that in the case of highly hydrophilic GO, variations in pH lead to significant physicochemical changes caused by deprotonation of oxygen moieties in GO. The laser reduction process results in the drastic removal of functional groups, turning the surface from hydrophilic (GO) to more hydrophobic (rGO). At the same time, this wetting change in rGO increases the water and mechanical stability while decreasing sensitivity to environmental

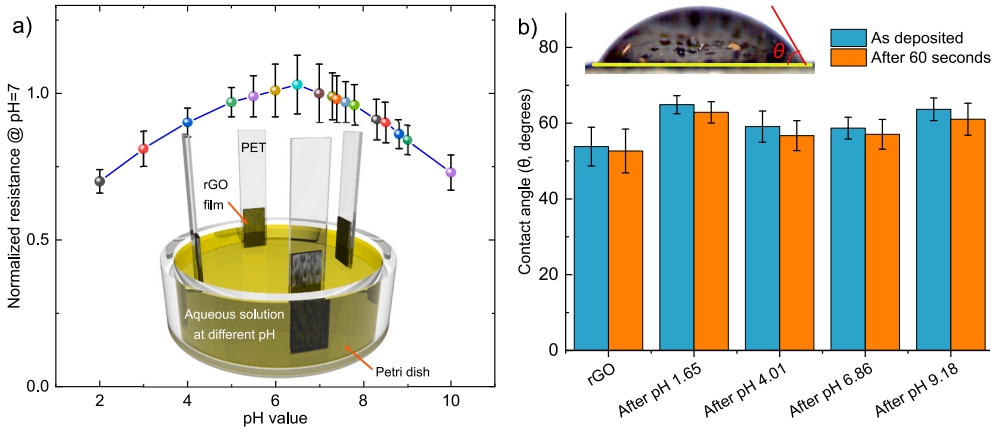


**Fig. 2.** Impedance change in solutions with different pH. The a) graph shows the range of the data obtained from four electrodes tested simultaneously normalized to the value at pH 7. The inset shows the electrode configuration used in these experiments. b) contact angle change after electrode stability test at different pH.

changes such as pH. Our experimental results showed that none of the pH levels from 1.65 to 9.18 influenced rGO surface wetting properties deduced from contact angle measurements (Fig. 2b). The average value of 60° did not shift, demonstrating the significant electrodes' stability to the external environment.

Although up to now, there is no precedent study on the stability of rGO bioelectrodes, the stability of rGO in electrochemical cells was reported before. Gao et al. showed 10 000 cycles of charging/recharging rGO based batteries with a 35% drop in capacitance (Gao et al., 2011) and even better with 84% stability after 4000 cycles (Tran et al., 2018). Moreover, Yun et al. demonstrated stable mechanical and electrical performance of rGO bioelectrodes with up to 5000 stretching cycles (Yun et al., 2017). Our results demonstrate that in addition to the mechanical stability reported before in those works, the pH and time stability of rGO bioelectrodes further supports their potential in wearable applications.

Raman spectroscopy is a key tool to analyze carbon nanomaterials and, in particular, to evaluate the degree of GO reduction (Ma et al., 2019). Here we use this tool to verify the chemical and structural stability of our rGO bioelectrodes. We are particularly interested in finding out if there are changes in substrate material and GO-covered PET in different buffer solutions with pH level varying from acidic to alkaline (pH 4.8, 5.2, 6, 8, and 9.2). Fig. S5a demonstrates that the Raman spectrum from PET does not change after immersion in solutions with different pH values. As for GO/PET, and rGO/PET (Fig. S5b and Fig. S5c, respectively), one can see the characteristic Raman modes for graphitic materials, D (1340 $cm^{-1}$) and G (1591 $cm^{-1}$) bands. The G peak refers to $E_{2g}$ graphite mode associated with the vibration of $sp^2$-hybridized carbon atoms. The D band is activated by Raman scattering with defects (Ma et al., 2019). In contrast to the case of GO spectra comparison at various pH values shown in Fig. S5b, the $I_D/I_G$ ratio differences for the rGO sample in Fig. S5c are at the noise level with no significant changes in peak positions. This result indicates that prolonged immersion in different acidic and basic solutions does not affect the rGO electrode structure. Notice that PET/GO and PET/rGO regions are investigated using different laser powers (1 mW and 4 mW, respectively). The reason is that GO could be easily reduced with powers higher than 1 mW, which would compromise the results. On the other hand, powers lower than 4 mW in the case of rGO lead to weaker signal intensity; therefore, measurements were obtained with the minimal possible power in both cases.

The thickness of the rGO layer is higher than that of GO, as estimated from SEM imaging results (Fig. S1). We noticed that GO was partially washed away after immersion in liquids with different pH. This is contrary to the case of rGO surfaces that remain intact after immersion. Moreover, by comparing SEM and optical images of initial surfaces and the ones kept in liquid media (Fig. 3), we observe that untreated surfaces have a rougher structure, which happens likely due to the removal of loosely bound top layers. The electrode immersed in NaCl solution shows salt crystals formed on its surface (Fig. 3), while there is no other difference between the samples soaked in buffers with pH 4.8 and pH 8. After immersion in solution with pH 9.2, the electrode shows a slight modification, having a lower extended surface. This surface morphology modification can be attributed to the compression of the double layer after ionization at high pH levels (Konkena and Vasudevan, 2012). However, these surface changes did not affect the electrical conductivity in any measurable way.

### 3.3. Interface modification

We were puzzled by the remarkable rGO bioelectrode stability in aqueous solutions at different pH discussed above. We hypothesized that except for the hydrophobic behavior there is something else into play, like for example, an enhanced interaction of rGO and PET, possibly resulting in composite formation. Such enhanced rGO/PET interaction could be investigated by studying other substrates besides PET. Moreover, we could expect a similar effect using other polymers with physicochemical properties close to PET. However, investigating rGO interactions with an entirely different polymer type could be more informative in terms of evidencing the impact of substrate properties. For this purpose, we chose Kapton as a substrate used for comparison purposes. Kapton is one of the most used substrates for flexible electronics and medical protective films (Kamyshny and Magdassi, 2019). Using GO films on Kapton, we reproduced the reduction process used for rGO/PET. By comparing with Kapton, we found that rGO/PET structure is more mechanically robust than rGO/Kapton or GO/PET. That was proven by the fact that on Kapton both rGO and GO layers were completely exfoliated after mechanical stripping by adhesive tape (Fig. 4 (a, b)). This result indicates poor mechanical stability and limits device applications; it is most likely explained by a higher melting point (270-400 °C compared to 250 °C for PET) that prevents laser-induced surface melting and partial integration with rGO. Contrary to those other material combinations, rGO on PET showed remarkable stability against mechanical stripping, for which only the top layer was removed (Fig. 4(c, d)). The improved adhesion and mechanical resistance strongly support the hypothesis of an rGO/PET composite formation, as recently reported for functionalized graphene films on PET (Rodriguez et al., 2020).

To visualize the modification of the underlying PET surface, the electrodes were sonicated for 2 min. The optical inspection (Fig. 4d) of the bare PET substrate shows surface structural changes due to the photothermal heating of PET and the formation of a laser-induced PET/rGO composite formation. One could also notice that the edges of the

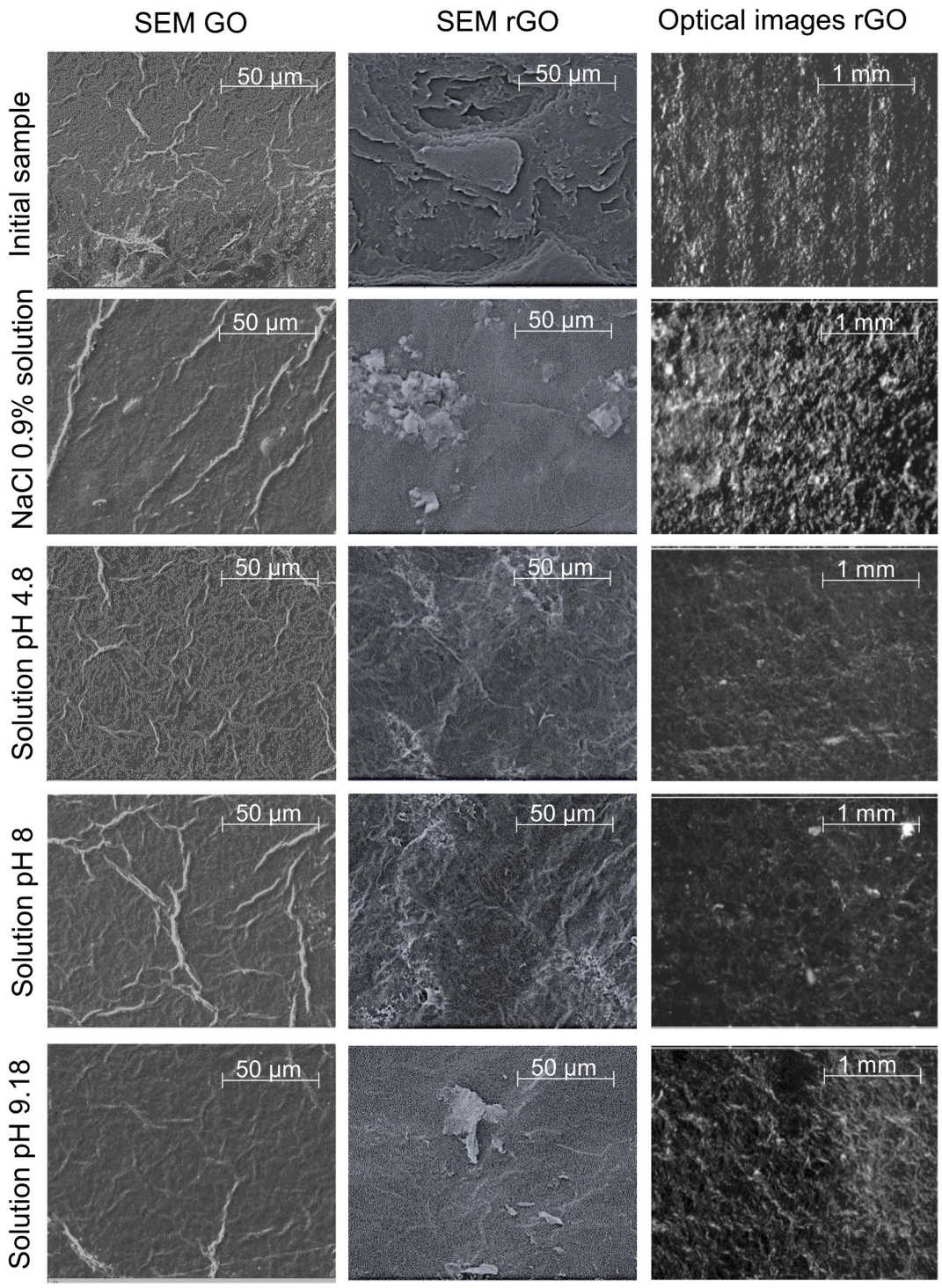


**Fig. 3.** SEM images of GO, rGO, and optical images of rGO after immersion in different media: NaCl 0.9% solution for two weeks; and buffer solutions with pH 4.8, pH 8, and pH 9.2 for 24 h.

reduced graphene oxide area are framed by melted PET appearing as a translucent film. No formation of a conductive carbonized layer is observed on PET after laser-irradiation without a GO layer which shows that the bioelectrode conductivity is entirely due to the rGO layer.

SEM and cross-sectional optical imaging analyses summarized in Fig. S3 shows no significant differences at the interface between PET and GO/rGO layers. We hypothesize that when exposed to laser radiation, the GO reduction occurs accompanied by a local temperature increase. The high temperature melts PET at the interface with rGO inducing the composite formation between these two materials. As a consequence, a strong PET/rGO film is formed that explains the remarkable electrode stability shown by adhesive tape stripping results. A similar effect was shown using a silicone substrate irradiated by a laser to create a flexible rGO electrode as a dielectric elastomer actuator (Kuhnel et al., 2019).

Our results are different from previous works on laser-reduced GO on PET, where no apparent adhesion between the two materials was reported when irradiated by 788 nm laser. The weak interaction between the two materials was such that it allowed rGO electrodes to be transferred by PDMS dry transfer (Strong et al., 2012). By increasing the laser energy using an fs laser at 515 nm Bobrinetskiy et al., showed that these

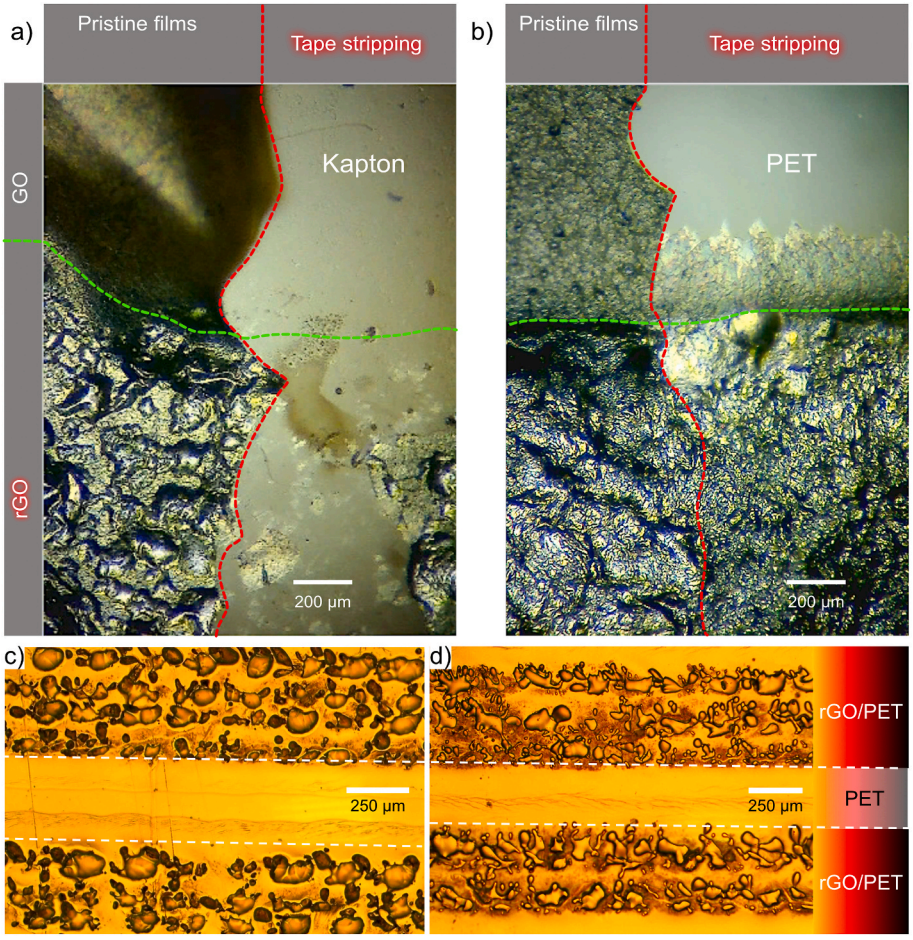


**Fig. 4.** Microscopy images at the horizontal interface between GO and rGO delimited by the green dashed lines on (a) Kapton and on (b) PET. The vertical interface marked by a red dashed line is with and without (left side) adhesive tape stripping. Optical images of rGO/GO on PET structure washed in water and (c) rubbed with a cotton disk and (d) for 2 min in an ultrasonic bath. (For interpretation of the references to color in this figure legend, the reader is referred to the Web version of this article.)

conditions resulted in rGO film detachment due to water evaporation and gas release (Bobrinetskiy et al., 2017). Those previous observations are contrary to our case that shows better adhesion between rGO and PET substrate. We attribute this higher adhesion to the laser irradiation conditions used in this work with a high power of 1W max and high energy of 3 eV (405 nm). These laser irradiation conditions can heat the rGO film and substrate up to the melting point of PET. Our results and interpretation of the higher adhesion of rGO/PET are in agreement with the work of Adelean et al. who showed that high energy laser irradiation (248 nm) of PET increased the adhesion with an Al film deposited by thermal evaporation (Ardelean et al., 2005). The authors demonstrate that the high-energy laser irradiation induces the formation of Al–O–C bonds at the film interface with PET, which is responsible for the higher adhesion observed in peel-off tests.

### 3.4. Cell proliferation tests

Besides electrical conductivity and mechanical stability, biocompatibility is another requirement of bioelectrodes. To investigate this point, the biocompatibility of rGO electrodes was investigated with fibroblasts proliferation tests using the blank PET substrate as a reference. Fig. 5 shows fluorescence microscopy imaging results of cells on PET and rGO surfaces. The insets in Fig. 5 show images of surfaces after washing cells away.

In the case of PET surface, the estimated amount of grown cells was 553 ± 150 units/mm$^2$, while for the rGO fibroblasts growth value was about 15% higher (640 ± 112 units/mm$^2$).

Moreover, the average resistance value of the rGO area before this test was 13.3 ± 6.6 kOhm, and increased to 50.2 ± 19.0 kOhm after the

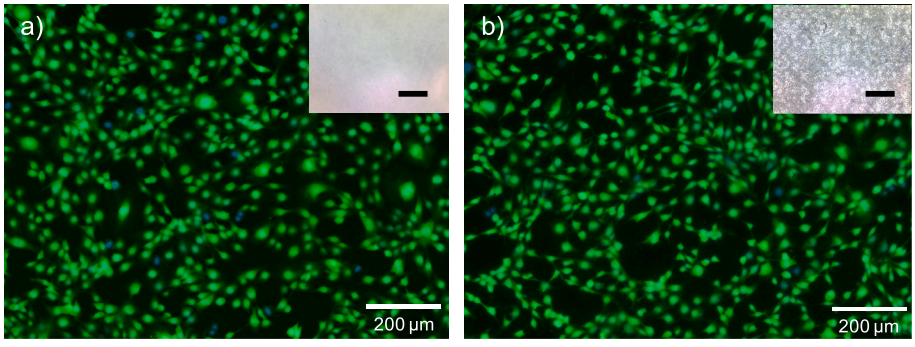


**Fig. 5.** Optical images of fibroblast cells grown on (a) PET and (b) rGO surfaces. The insets show the surfaces after cells were washed away. The insets scale bar is 500 μm.

test. We attribute this change in resistance to partial delamination of the top rGO layer during the washing process. Even though it deserves noticing that the external environment did not affect the material performance and its mechanical stability. The changes in absolute resistance values in kOhm range do not drastically influence the bioelectrode performance.

### 3.5. *In vivo* study

GO and rGO dispersion stability is reduced in the presence of higher ionic valence solutions (Chowdhury et al., 2015), and it is also affected by the presence of organic matter (sweat, bacteria, skin cells, *etc.*). Therefore, in addition to stability investigations in pH buffer solutions, it is essential to evaluate the influence of a patient's sweat in the performance of our rGO bioelectrodes. For a long-time stability test, a volunteer wore a setup made of three rGO electrodes and one Ag/AgCl attached according to Wilson's scheme (AlGhatrif and Lindsay, 2012). The same scheme is used in commercially available equipment like Holter monitors commonly used in electrocardiography.Fig.6shows a summary of our ECG recordingsobtained during the 108 h test. Unlike 1-day monitoring, this 108h time window is sufficient for a clinician to detect most heart rate abnormalities. The interval between measurement was 12 h. Commercial Ag/AgCl electrodes showed a tendency to get dry with time and thus they were replaced with new ones (same batch and same package) after 36 and 72 h of constant measurement. In Fig. 6c one could notice that after 40 h, Ag/AgCl electrodes electrical impedance increased. This impedance increase occurs because after electrode replacement some time is required to reach electrochemical equilibrium between the skin and the electrode. Meanwhile, for rGO electrodes, the replacement was not necessary and the impedance values remained the same during the whole test period. Even though the data obtained at 40 and 80 h of recording contact impedance for Ag/AgCl electrodes is higher than for rGO ones, it does not affect the results as the signal quality remains high. Even though 40–80 h recording contact impedance for Ag/AgCl electrodes is higher than for rGO ones, it does not affect the results as the signal quality remains high. However, conventional electrode replacement was necessary not only for the sake of keeping the signal quality but also for ethical reasons for this *in vivo* study. Following ethical guideline recommendations, after continuous use for a period varying from 24 to 72 h, we should either stop monitoring completely or replace the deteriorated electrodes and provide appropriate measures to eliminate skin irritation of the volunteer. Let us also highlight that it was not our aim to demonstrate the superiority of new rGO electrodes over Ag/AgCl for long-term use, but rather to prove their state-of-the-art performance over a more extended period. High-quality Ag/AgCl electrodes when used according to the manufacturer's specifications have almost unbeatable electrical parameters (low noise and contact impedance). Our new rGO bioelectrodes provide comparable characteristics for at least 108 hrs.

To put in perspective the performance of our electrodes, we compiled some characteristics and usability (measured in hours) of bioelectrode materials commercially available up to this date. While some electrodes have the usability of 72h, most electrodes have 24h usability, and at 108h, our electrodes show the longest usability without the need for any additional contacting material (see Table S1 in the Supplementary Information). The comparative data obtained from commercial and rGO bioelectrodes presented in Fig. 6aallows obtaining the time between peaks related to heart rate. Fig. 6b shows the comparison of the induced high-frequency noise and useful signal. These results demonstrate the remarkable sensitivity of dry rGO electrodes with respect to the state-of-the-art ones. We also evaluated the correlation function between two types of electrodes (Fig. 6d), indicating that we achieved a remarkable signal match with over 98% fidelity. High-magnification SEM images further confirm that the surface of rGO-bioelectrode did not react with skin cells or other organic fluids during the *in vivo* study. Fig. 6f and 6g shows two different areas of the same electrode after the 108 h test experiment with no structural changes or the presence of organic matter.

It is worth noticing the remarkable high impedance stability of dry bioelectrodes observed for reduced graphene oxide in an aggressive environment (constantly changing the level of acidity, bending of the surface, and the influence of microflora), while maintaining a performance similar to commercial Ag/AgCl electrodes. Considering the

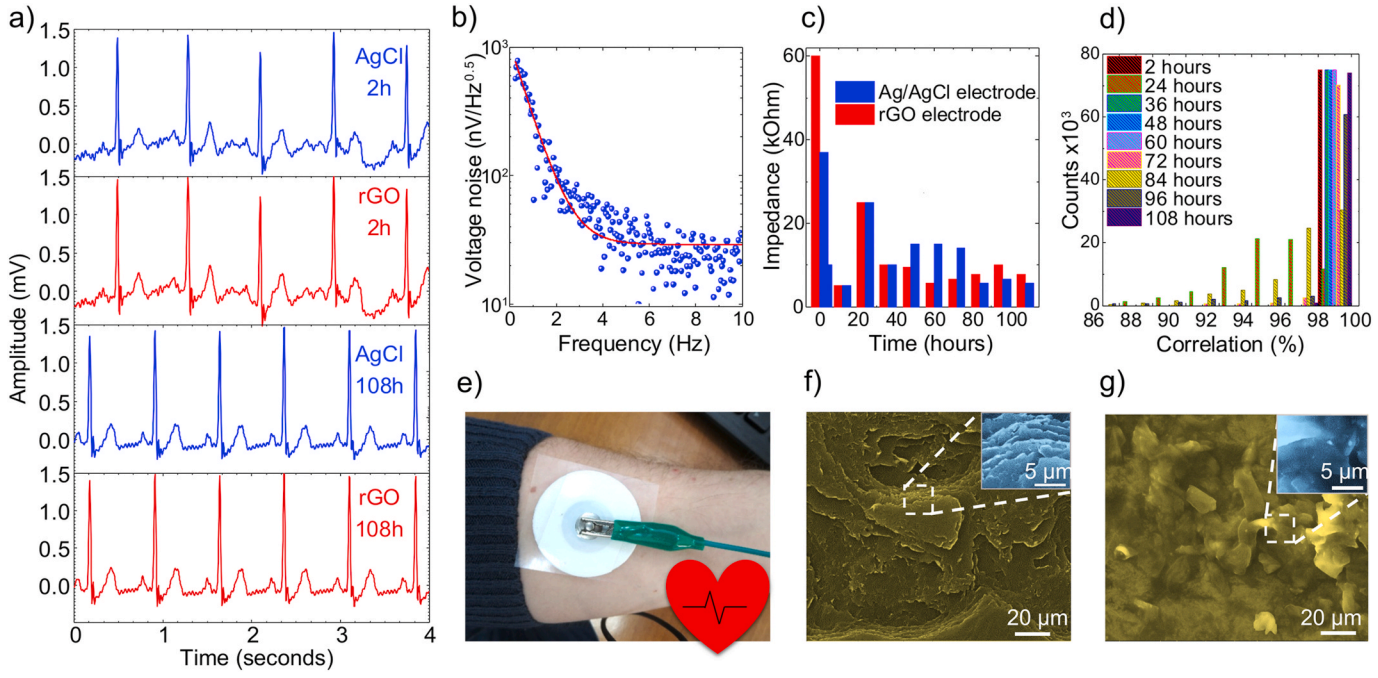


**Fig. 6.** ECG processed data: a) the ECG signals with rGO bioelectrode compared to the Ag/AgCl electrode at different measurement times; b) voltage noise *vs.* frequency; c) the bioimpedance change of skin-electrode contact during the test; d) signal correlation from different electrodes with 5 min ECG data at different times (over 98% match obtained). (e) An actual photograph of the rGO bioelectrode worn by a volunteer. SEM images of rGO bioelectrodes f) before and g) after 108 h continuously in contact with human skin after the *in vivo* study.

superb performance of our bioelectrodes, and especially the results of our *in vivo* study, we now established the potential to perform long-term clinical studies for heart disease detection with the implementation of the rGO-based technology demonstrated in this work.

## 4. Conclusions

Following our concept illustrated in Fig. 1, we demonstrate an innovative application of laser-reduced GO as skin bioelectrodes. Our rGO devices remain intact in aggressive environments that mimic physiological conditions. This implies that our electrodes pose promising applications where long-term wearing on the human body is required. The bioelectrodes are chemically stable as proven by Raman spectroscopy that showed the negligible changes in the chemical composition of the rGO electrodes surface after prolonged immersion in solutions with different pH. Furthermore, the remarkable mechanical stability of rGO bioelectrodes was demonstrated under stringent conditions in an ultrasonic bath. The mechanical and chemical robustness, as well as the water stability of rGO bioelectrodes, are attributed to effects from laser irradiation that induces an rGO-PET composite formation. *In vivo* ECGinvestigations comparing rGO bioelectrodes and commercially-available Ag/AgCl electrodes showed the advantages of our graphene-based technology with respect to conventional bioelectrodes. This competitiveness is further illustrated by several benefits over incumbent technology, including long-term operation and the ability to use rGO bioelectrodes without the need for any gel electrolyte. Moreover, taking into account the state of the art technology and our experimental results, it is possible to use other substrates besides PET, including highly flexible ones (*e.g.;* PDMS) to increase the shape conformity of electrodes to the skin. This competitive laser-graphene technology is not only superior in measurement stability but also inexpensive, compatible with flexible electronics and large-scale solution-processable manufacture that incentivize its widespread implementation in clinical venues.

## CRediT authorship contribution statement

**G. Murastov:** Conceptualization, Investigation, Validation, Formal analysis, Visualization, Supervision, Writing - original draft, Writing - review & editing. **E. Bogatova:** Investigation, Formal analysis, Writing - original draft, Writing - review & editing. **K. Brazovskiy:** Conceptualization, Methodology, Software, Writing - original draft, Writing - review & editing, Resources. **I. Amin:** Writing - original draft, Writing - review & editing. **A. Lipovka:** Formal analysis, Writing - original draft, Writing - review & editing. **E. Dogadina:** Investigation, Writing - original draft. **A. Cherepnyov:** Investigation, Writing - original draft. **A. Ananyeva:** Investigation, Formal analysis. **E. Plotnikov:** Investigation, Formal analysis, Writing - original draft, Writing - review & editing. **V. Ryabov:** Conceptualization, Writing - original draft. **R.D. Rodriguez:** Conceptualization, Methodology, Visualization, Supervision, Writing - original draft, Writing - review & editing. **E. Sheremet:** Validation, Supervision, Writing - original draft, Writing - review & editing, Resources, Funding acquisition.

## Declaration of competing interest

The authors declare that they have no known competing financial interests or personal relationships that could have appeared to influence the work reported in this paper.

## Acknowledgment

We thank Mohamed M. Chehimi and Pavel S. Postnikov for assistance with the XPS experiments and Kostikova Larisa Anatolyevna for IR experiments. This research is supported by the Tomsk Polytechnic University within the framework of the Tomsk Polytechnic University Competitiveness Enhancement Program (VIU-RSHEP-198/2020).

## Appendix A. Supplementary data

Supplementary data to this article can be found online at https://doi.org/10.1016/j.bios.2020.112426.

## References

AlGhatrif, M., Lindsay, J., 2012. A brief review: history to understand fundamentals of electrocardiography. J. Community Hosp. Intern. Med. Perspect. 2 https://doi.org/10.3402/jchimp.v2i1.14383.

Al-Hamry, A., Kang, H., Sowade, E., Dzhagan, V., Rodriguez, R.D., Müller, C., Zahn, D.R.T., Baumann, R.R., Kanoun, O., 2016. Tuning the reduction and conductivity of solution-processed graphene oxide by intense pulsed light. Carbon N. Y. 102, 236–244.

Ardelean, H., Petit, S., Laurens, P., Marcus, P., Arefi-Khonsari, F., 2005. Effects of different laser and plasma treatments on the interface and adherence between evaporated aluminium and polyethylene terephthalate films: X-ray photoemission, and adhesion studies. Appl. Surf. Sci. 243, 304–318.

Ask, P., Oberg, P.A., Odman, S., Tenland, T., Skogh, M., 1979. ECG electrodes. A study of electrical and mechanical long-term properties. Acta Anaesthesiol. Scand. 23, 189–206.

Beutler, B.D., al, E.. n.d. Localized cutaneous argyria: report of two patients and literature review. - PubMed - NCBI [WWW Document]. https://www.ncbi.nlm.nih.gov/pubmed/28329568, 6.20.19.

Bobrinetskiy, I.I., Emelianov, A.V., Smagulova, S.A., Komarov, I.A., Otero, N., Romero, P.M., 2017. Laser direct 3D patterning and reduction of graphene oxide film on polymer substrate. Mater. Lett. https://doi.org/10.1016/j.matlet.2016.10.073.

Casson, A.J., Saunders, R., Batchelor, J.C., 2017. Five day attachment ECG electrodes for longitudinal bio-sensing using conformal tattoo substrates. IEEE Sensor. J. 17, 2205–2214.

(Chair), B.G., (co-chair), A.P., Benjamin, E.J., Boriani, G., Crijns, H.J., Fogel, R.I., Van Gelder, I.C., Halle, M., Kudaiberdieva, G., Lane, D.A., Larsen, T.B., Lip, G.Y.H., Løchen, M.-L., Marin, F., Niebauer, J., Sanders, P., Tokgozoglu, L., Vos, M.A., Van Wagoner, D.R., Fauchier, L., Savelieva, I., Goette, A., Agewall, S., Chiang, C.-E., Figueiredo, M., Stiles, M., Dickfeld, T., Patton, K., Piepoli, M., Corra, U., Marques-Vidal, P.M., Faggiano, P., Schmid, J.-P., Abreu, A., reviewers, D., 2017. European heart rhythm association (EHRA)/European association of cardiovascular prevention and rehabilitation (EACPR) position paper on how to prevent atrial fibrillation endorsed by the heart rhythm society (HRS) and asia pacific heart rhythm society (APHRS). Eur. J.Prev. Cardiol. https://doi.org/10.1177/2047487316676037.

Chen, G., Li, Y., Bick, M., Chen, J., 2020. Smart textiles for electricity generation. Chem. Rev. 120, 3668–3720.

Chlaihawi, A.A., Narakathu, B.B., Emamian, S., Bazuin, B.J., Atashbar, M.Z., 2018. Development of printed and flexible dry ECG electrodes. Sensing and Bio-Sensing Research. https://doi.org/10.1016/j.sbsr.2018.05.001.

Chowdhury, I., Mansukhani, N.D., Guiney, L.M., Hersam, M.C., Bouchard, D., 2015. Aggregation and stability of reduced graphene oxide: complex roles of divalent cations, pH, and natural organic matter. Environ. Sci. Technol. 49, 10886–10893.

Dedelaite, L., Rodriguez, R.D., Andriukonis, E., Hietschold, M., Zahn, D.R.T., Ramanavicius, A., 2018. Surfaces functionalized by graphene oxide nanosheets for single cell investigations. Sensor. Actuator. B Chem. 255, 1735–1743.

D'Souza, O.J., Mascarenhas, R.J., Satpati, A.K., Basavaraja, B.M., 2019. A novel ZnO/reduced graphene oxide and Prussian blue modified carbon paste electrode for the sensitive determination of Rutin. Sci. China Chem. https://doi.org/10.1007/s11426-018-9353-x.

Eda, G., Fanchini, G., Chhowalla, M., 2008. Large-area ultrathin films of reduced graphene oxide as a transparent and flexible electronic material. Nat. Nanotechnol. 3, 270–274.

Gan, D., Huang, Z., Wang, X., Jiang, L., Wang, C., Zhu, M., Ren, F., Fang, L., Wang, K., Xie, C., Lu, X., 2020. Graphene oxide-templated conductive and redox-active nanosheets incorporated hydrogels for adhesive bioelectronics. Adv. Funct. Mater. https://doi.org/10.1002/adfm.201907678.

Gao, W., Singh, N., Song, L., Liu, Z., Reddy, A.L.M., Ci, L., Vajtai, R., Zhang, Q., Wei, B., Ajayan, P.M., 2011. Direct laser writing of micro-supercapacitors on hydrated graphite oxide films. Nat. Nanotechnol. 6, 496–500.

Gladstone, D.J., Spring, M., Dorian, P., Panzov, V., Thorpe, K.E., Hall, J., Vaid, H., O'Donnell, M., Laupacis, A., Côté, R., Sharma, M., Blakely, J.A., Shuaib, A., Hachinski, V., Coutts, S.B., Sahlas, D.J., Teal, P., Yip, S., Spence, J.D., Buck, B., Verreault, S., Casaubon, L.K., Penn, A., Selchen, D., Jin, A., Howse, D., Mehdiratta, M., Boyle, K., Aviv, R., Kapral, M.K., Mamdani, M., 2014. Atrial fibrillation in patients with cryptogenic stroke. EMBRACE Investigators and Coordinators N. Engl. J. Med. 370, 2467–2477.

Gruetzmann, A., Hansen, S., Müller, J., 2007. Novel dry electrodes for ECG monitoring. Physiol. Meas. 28, 1375–1390.

Gugoasa, L.A., Staden, R.-I.S., van Staden, J.F., Coroș, M., Pruneanu, S., 2019. Electrochemical determination of bisphenol A in saliva by a novel three-dimensional (3D) printed gold-reduced graphene oxide (rGO) composite paste electrode. Anal. Lett. https://doi.org/10.1080/00032719.2019.1620262.

Guo, K., Qian, K., Zhang, S., Kong, J., Yu, C., Liu, B., 2011. Bio-electrocatalysis of NADH and ethanol based on graphene sheets modified electrodes. Talanta 85, 1174–1179.

Guo, L., Hao, Y.-W., Li, P.-L., Song, J.-F., Yang, R.-Z., Fu, X.-Y., Xie, S.-Y., Zhao, J., Zhang, Y.-L., 2018. Improved NO gas sensing properties of graphene oxide reduced by two-beam-laser interference. Sci. Rep. 8, 4918.
Kaitainen, S., Kutvonen, A., Suvanto, M., Pakkanen, T.T., Lappalainen, R., Myllymaa, S., 2014. Liquid silicone rubber (LSR)-based dry bioelectrodes: the effect of surface micropillar structuring and silver coating on contact impedance. Sens. Actuators A Phys. 206, 22–29.
Kamyshny, A., Magdassi, S., 2019. Conductive nanomaterials for 2D and 3D printed flexible electronics. Chem. Soc. Rev. 48, 1712–1740.
Karimi, A., Othman, A., Uzunoglu, A., Stanciu, L., Andreescu, S., 2015. Graphene based enzymatic bioelectrodes and biofuel cells. Nanoscale 7, 6909–6923.
Konkena, B., Vasudevan, S., 2012. Understanding aqueous dispersibility of graphene oxide and reduced graphene oxide through pKa measurements. J. Phys. Chem. Lett. 3, 867–872.
Kuhnel, D.T., Rossiter, J.M., Faul, C.F.J., 2019. Laser-Scribed graphene oxide electrodes for soft electroactive devices. Advanced Materials Technologies. https://doi.org/10.1002/admt.201800232.
Lee, C.-S., Yu, S.H., Kim, T.H., 2017. One-step electrochemical fabrication of reduced graphene oxide/gold nanoparticles nanocomposite-modified electrode for simultaneous detection of dopamine, ascorbic acid, and uric acid. Nanomaterials (Basel) 8. https://doi.org/10.3390/nano8010017.
Lipovka, A., Rodriguez, R., Bolbasov, E., Maryin, P., Tverdokhlebov, S., Sheremet, E., 2020. Time-stable wetting effect of plasma-treated biodegradable scaffolds functionalized with graphene oxide. Surf. Coating. Technol. 388, 125560.
Li, S., Cheng, C., Thomas, A., 2017. Carbon-based microbial-fuel-cell electrodes: from conductive supports to active catalysts. Adv. Mater. 29 https://doi.org/10.1002/adma.201602547.
Liu, Z., Ma, Y., Ouyang, H., Shi, B., Li, N., Jiang, D., Xie, F., Qu, D., Zou, Y., Huang, Y., Li, H., Zhao, C., Tan, P., Yu, M., Fan, Y., Zhang, H., Wang, Z.L., Li, Z., 2019. Transcatheter self-powered ultrasensitive endocardial pressure sensor. Adv. Funct. Mater. 29, 1807560.
Li, Y., Zhang, P., Du, Q., Peng, X., Liu, T., Wang, Z., Xia, Y., Zhang, W., Wang, K., Zhu, H., Wu, D., 2011. Adsorption of fluoride from aqueous solution by graphene. J. Colloid Interface Sci. 363, 348–354.
Ma, B., Rodriguez, R.D., Ruban, A., Pavlov, S., Sheremet, E., 2019. The correlation between electrical conductivity and second-order Raman modes of laser-reduced graphene oxide. Phys. Chem. Chem. Phys. 21, 10125–10134.
Maiti, D., Tong, X., Mou, X., Yang, K., 2018. Carbon-based nanomaterials for biomedical applications: a recent study. Front. Pharmacol. 9, 1401.
Meng, K., Zhao, S., Zhou, Y., Wu, Y., Zhang, S., He, Q., Wang, X., Zhou, Z., Fan, W., Tan, X., Yang, J., Chen, J., 2020. A wireless textile-based sensor system for self-powered personalized health care. Matter. https://doi.org/10.1016/j.matt.2019.12.025.
Ouyang, H., Tian, J., Sun, G., Zou, Y., Liu, Z., Li, H., Zhao, L., Shi, B., Fan, Y., Fan, Y., Wang, Z.L., Li, Z., 2017. Self-powered pulse sensor for antidiastole of cardiovascular disease. Adv. Mater. 29 https://doi.org/10.1002/adma.201703456.
Paton, K.R., Varrla, E., Backes, C., Smith, R.J., Khan, U., O'Neill, A., Boland, C., Lotya, M., Istrate, O.M., King, P., Higgins, T., Barwich, S., May, P., Puczkarski, P., Ahmed, I., Moebius, M., Pettersson, H., Long, E., Coelho, J., O'Brien, S.E., McGuire, E.K., Sanchez, B.M., Duesberg, G.S., McEvoy, N., Pennycook, T.J., Downing, C., Crossley, A., Nicolosi, V., Coleman, J.N., 2014. Scalable production of large quantities of defect-free few-layer graphene by shear exfoliation in liquids. Nat. Mater. 13, 624–630.
Pedrosa, P., Alves, E., Barradas, N.P., Martin, N., Fiedler, P., Haueisen, J., Vaz, F., Fonseca, C., 2014. Electrochemical behaviour of nanocomposite Agx:TiN thin films for dry biopotential electrodes. Electrochim. Acta 125, 48–57.
Robinson, J.T., Keith Perkins, F., Snow, E.S., Wei, Z., Sheehan, P.E., 2008. Reduced graphene oxide molecular sensors. Nano Lett. https://doi.org/10.1021/nl8013007.
Rodriguez, R.D., Khalelov, A., Postnikov, P.S., Lipovka, A., Dorozhko, E., Amin, I., Murastov, G.V., Chen, J.-J., Sheng, W., Trusova, M.E., Chehimi, M.M., Sheremet, E., 2020. Beyond graphene oxide: laser engineering functionalized graphene for flexible electronics. Mater. Horiz. 119, 5461.
Rodriguez, R.D., Murastov, G.V., Lipovka, A., Fatkullin, M.I., Nozdrina, O., Pavlov, S.K., Postnikov, P.S., Chehimi, M.M., Chen, J.-J., Sheremet, E., 2019. High-power laser-patterning graphene oxide: a new approach to making arbitrarily-shaped self-aligned electrodes. Carbon. https://doi.org/10.1016/j.carbon.2019.05.049.
Sanna, T., Diener, H.-C., Passman, R.S., Di Lazzaro, V., Bernstein, R.A., Morillo, C.A., Rymer, M.M., Thijs, V., Rogers, T., Beckers, F., Lindborg, K., Brachmann, J., 2014. Cryptogenic stroke and underlying atrial fibrillation. N. Engl. J. Med. https://doi.org/10.1056/nejmoa1313600.
Scheman, A., Hylwa-Deufel, S., Jacob, S.E., Katta, R., Nedorost, S., Warshaw, E., Eifrid, K., Geiser, A.J., McGaughey, L., Scheman, N., Kimyon, R., Rundle, C., Shaver, R., 2019. Alternatives for allergens in the 2018 American contact dermatitis society core series: report by the American contact alternatives group. Dermatitis 30, 87–105.
Searle, A., Kirkup, L., 2000. A direct comparison of wet, dry and insulating bioelectric recording electrodes. Physiol. Meas. https://doi.org/10.1088/0967-3334/21/2/307.
Shahandashti, P.F., Pourkheyrollah, H., Jahanshahi, A., Ghafoorifard, H., 2019. Highly conformable stretchable dry electrodes based on inexpensive flex substrate for long-term biopotential (EMG/ECG) monitoring. Sensor Actuator Phys. https://doi.org/10.1016/j.sna.2019.06.041.
Steinberg, C., Philippon, F., Sanchez, M., Fortier-Poisson, P., O'Hara, G., Molin, F., Sarrazin, J.-F., Nault, I., Blier, L., Roy, K., Plourde, B., Champagne, J., 2019. A novel wearable device for continuous ambulatory ECG recording: proof of concept and assessment of signal quality. Biosensors 9. https://doi.org/10.3390/bios9010017.
Strankowski, M., Włodarczyk, D., Piszczyk, Ł., Strankowska, J., 2016. Polyurethane nanocomposites containing reduced graphene oxide, FTIR, Raman, and XRD studies. Journal of Spectroscopy. https://doi.org/10.1155/2016/7520741.
Strong, V., Dubin, S., El-Kady, M.F., Lech, A., Wang, Y., Weiller, B.H., Kaner, R.B., 2012. Patterning and electronic tuning of laser scribed graphene for flexible all-carbon devices. ACS Nano 6, 1395–1403.
Taniselass, S., Md Arshad, M.K., Gopinath, S.C.B., 2019. Graphene-based electrochemical biosensors for monitoring noncommunicable disease biomarkers. Biosens. Bioelectron. https://doi.org/10.1016/j.bios.2019.01.047.
Tiwari, A., 2017. Graphene Bioelectronics. Elsevier Science.
Tran, T.X., Choi, H., Che, C.H., Sul, J.H., Kim, I.G., Lee, S.-M., Kim, J.-H., In, J.B., 2018. Laser-induced reduction of graphene oxide by intensity-modulated line beam for supercapacitor applications. ACS Appl. Mater. Interfaces 10, 39777–39784.
Uter, W., Werfel, T., White, I.R., Johansen, J.D., 2018. Contact allergy: a review of current problems from a clinical perspective. Int. J. Environ. Res. Publ. Health 15. https://doi.org/10.3390/ijerph15061108.
Wang, X., Liu, A., Xing, Y., Duan, H., Xu, W., Zhou, Q., Wu, H., Chen, C., Chen, B., 2018. Three-dimensional graphene biointerface with extremely high sensitivity to single cancer cell monitoring. Biosens. Bioelectron. 105, 22–28.
Bioelectrodes. In: Webster, J.G. (Ed.), 2006. Encyclopedia of Medical Devices and Instrumentation, Electrode Impedance and Voltage Offset as They Affect Efficacy and Accuracy of VCG and ECG Measurements. John Wiley & Sons, Inc., Hoboken, NJ, USA, p. 210.
Yun, Y.J., Ju, J., Lee, J.H., Moon, S.-H., Park, S.-J., Kim, Y.H., Hong, W.G., Ha, D.H., Jang, H., Lee, G.H., Chung, H.-M., Choi, J., Nam, S.W., Lee, S.-H., Jun, Y., 2017. Highly elastic graphene-based electronics toward electronic skin. Adv. Funct. Mater. 27, 1701513.
Zhang, N., Huang, F., Zhao, S., Lv, X., Zhou, Y., Xiang, S., Xu, S., Li, Y., Chen, G., Tao, C., Nie, Y., Chen, J., Fan, X., 2020. Photo-rechargeable fabrics as sustainable and robust power sources for wearable bioelectronics. Matter. https://doi.org/10.1016/j.matt.2020.01.022.
Zhang, T., Rodriguez, R.D., Amin, I., Gasiorowski, J., Rahaman, M., Sheng, W., Kalbacova, J., Sheremet, E., Zahn, D.R.T., Jordan, R., 2018. Bottom-up fabrication of graphene-based conductive polymer carpets for optoelectronics. J. Mater. Chem. C. https://doi.org/10.1039/c8tc00554k.
Zhou, W., Song, R., Pan, X., Peng, Y., Qi, X., Peng, J., Hui, K.S., Hui, K.N., 2013. Fabrication and impedance measurement of novel metal dry bioelectrode. Sensor Actuator Phys. https://doi.org/10.1016/j.sna.2013.06.025.
Zhou, Z., Padgett, S., Cai, Z., Conta, G., Wu, Y., He, Q., Zhang, S., Sun, C., Liu, J., Fan, E., Meng, K., Lin, Z., Uy, C., Yang, J., Chen, J., 2020. Single-layered ultra-soft washable smart textiles for all-around ballistocardiograph, respiration, and posture monitoring during sleep. Biosens. Bioelectron. 155, 112064.
Zou, Y., Tan, P., Shi, B., Ouyang, H., Jiang, D., Liu, Z., Li, H., Yu, M., Wang, C., Qu, X., Zhao, L., Fan, Y., Wang, Z.L., Li, Z., 2019. A bionic stretchable nanogenerator for underwater sensing and energy harvesting. Nat. Commun. 10, 2695.